Supplementary Information for

From Waste to Energy and Fuel: Novel Cu_xNi_y/CN catalysts from waste melamine resin for efficient nitrate reduction to ammonia

Feng Gong[*a], Shaohuan Hong[a], Jiaming Song[a], Chaozhen Liu[b], Shenglin Liu[a], Junjie Feng[a], Qingwen Wu[a], Yonglian Xiong[c], Ljiljana Medic-Pejic[d], Yuan Cheng[e, f], and Zhiqi Zhang[*a]

[a] Key Laboratory of Energy Thermal Conversion and Control of Ministry of Education, School of Energy and Environment, Southeast University, Nanjing, 211189, Jiangsu, China

[b] State Key Laboratory of Clean Energy Utilization, Zhejiang University, Hangzhou 310027, China

[c] College of Automotive Engineering, Yancheng Institute of Technology, Yancheng City, Jiangsu 224051, PR China

[d] Department of Energy and Fuels, E.T.S. Ingenieros de Minas y Energía, Universidad Politécnica de Madrid, Ríos Rosas 21, 28003, Madrid, Spain

[e] Suzhou Industrial Park Monash Research Institute of Science and Technology, Monash University, Suzhou 215000, China

[f] Department of Materials Science and Engineering, Monash University, Clayton, VIC 3800, Australia

[*] Corresponding author. E-mail address: gongfeng@seu.edu.cn (F.G.) and zhangzhiqi@seu.edu.cn (Z.Z.).

Experimental Section

Chemicals

$Cu(NO_3)_2 \cdot 3H_2O$ (99%), $Ni(NO_3)_2 \cdot 6H_2O$ (98%) and potassium nitrate (GR,99.0%) from Aladdin, potassium hydroxide (99.99% metals basis) from MACKLIN, deionized water (18.25 MΩ cm resistivity) obtained via an ultrapure water equipment, sodium citrate (98%) from Leyan, salicylic acid (≥99.5%) from Sinopharm, sodium hypochlorite (available chlorine ≥20%) from MACKLIN and sodium nitrosoferricyanide (99.0%) from Aladdin were used in the experiments.

Cu_xNi_y/CN catalysts and electrodes preparation

A waste melamine resin block (3×3×1 cm^3) was dropped into 1 M KOH solution. A certain amount of $Cu(NO_3)_2 \cdot 3H_2O$ and $Ni(NO_3)_2 \cdot 6H_2O$ were dissolved in deionized water at room temperature to simulate electroplating wastewater. After the saturated absorption of the melamine resin, the copper and nickel nitrate mixture were filtered by saturated blocks, within which an aquamarine blue color would be observed to be $Cu(OH)_2$ and $Ni(OH)_2$ deposition. Attributed to the porous structure of melamine resin, the precipitation could be held in the block and consequently NO_3^- would be allowed to leave. Before calcining, the melamine resin block full of precipitation was repeatedly washed to neutral, as the alkaline and acid residues would influence the process of calcining and alloying. The calcining process was conducted under H_2/Ar (5 vol% H_2) atmosphere at 550℃ with a 5 ℃/min heating rate.

Characterization of Cu_xNi_y/CN catalysts

X-ray diffraction (XRD) was used to analyze the crystal structure of the catalyst. XRD patterns of the catalysts were collected using Rigaku UltimaIV with a Cu target, a voltage of 40 V, and a current of 40 mA. X-ray photoelectron spectroscopy (XPS) was carried out on an ESCALAB 250Xi spectrometer (Thermo Fisher Scientific, USA), which has an Al Kα X-ray (hν=1486.65 eV) source and a pass energy of 30 eV with a

power of 100 W (10 kV and 10 mA), and all of the binding energies were calibrated with the binding energy of C1s at 284.6 eV. Every sample was examined at a pressure lower than 1.0×10^{-9} Pa. With a step of 0.05 eV, spectra were collected using the Avantage software (Version 5.979). A field-emission scanning electron microscope (SEM) was executed by the Hitachi SU-8220 instrument. Transmission electron microscopy (TEM) was carried out on a FEI F20 TWIN instrument. Energy dispersion X-ray (EDX) was carried out on a JEM 2100f.

Preparing the cathode with CuxNiy/CN catalysts loaded and electrocatalytic reduction of nitrate

Carbon paper (CP) was selected as the substrate for catalysts. A mixture of prepared Cu_xNi_y/CN (6 mg), 5 wt% nafion (50 μL) and ethanol (550 μL) was formed in catalyst ink under ultrasonic for 40 min. In the mixture, the loading mass of catalyst was normalized by its concentration, which was estimated by the volume dropped on the CP. After being coated on the carbon paper, the prepared cathode was dried at room temperature for 30 min. The NO_3^-RR tests were performed in an H-type electrolytic cell filled with KNO_3 and 1.0 M KOH as the electrolyte. A three-electrode system was employed for the tests with the prepared cathode loaded Cu_xNi_y/CN catalysts, platinum electrode (1×1 cm^2), and Ag/AgCl electrode as the working, counter, and reference electrodes, respectively. The Pt plate was selected for its inertia in NO_3^-RR. The linear sweep voltammetry (LSV) and electrolysis tests were performed on a CHI 760 electrochemical workstation. Before the electrochemical test, oxygen was removed by bubbling high-purity Ar through the solution for 20 min. LSV was carried out in 1.0 M KOH with or without certain concentration of KNO_3 at a scan rate of 5 mV s^{-1}. After electrochemical experiments, 2 mL of solution was taken out to analyze the concentration of NH_4^+.

Determination of ammonia

A UV-Vis spectrophotometer was used to analyze the concentration of NH_4^+-N.

The amount of ammonia was detected by the indophenol blue method. 2 mL of electrolyte after the experiment was taken out for analysis. Then 2 mL of solution A, 1 mL of solution B, and 0.2 mL of solution C were mixed with the sample. Solution A is composed of 4.0 g NaOH, 5.77 g salicylic acid, 5.77 g sodium citrate, and 100 ml deionized water. Solution B is NaClO (available chlorine, 4.0 wt%). Solution C is obtained by dissolving 0.2 g of sodium nitrosoferricyanide in 20 mL of water. After 2 h under ambient conduction, the UV-Vis absorption spectrum was recorded, and the absorbance value was obtained at the wavelength of 655 nm. The standard NH_4^+ solutions with the given concentrations of NH_4Cl in 1.0 M KOH were prepared for building the calibration curve.

Faradaic efficiency and ammonia yield rate

The ammonia yield rate was calculated through the concentration of NH_4^+, reaction time, and mass of catalyst, according to Eq. (1). And the faradaic efficiency was determined from the electric charge consumed for producing ammonia and the total charge passed through the electrode according to Eqs. (2) and (3).

$$Ammonia\ yield\ rate = \frac{C_{NH_3} \times V}{m_{cat.} \times t} \tag{1}$$

$$Faradaic\ efficiency = \frac{8F \times C_{NH_3} \times V}{M_{NH_3} \times Q} \times 100\% \tag{2}$$

$$Q = \iint didt \tag{3}$$

where C_{NH_3} represents the mass concentration of NH_3, V is the volume of electrolyte (40 mL), $m_{cat.}$ is the mass of catalysts on carbon paper, t is the reaction time, M_{NH_3} is the molar mass of NH_3, F is the Faradaic constant (96485 C mol^{-1}), and Q is the total charge passing through the cathode. Additionally, i represents the current under certain potential.

Density functional theory calculations

The spin-polarized density functional theory (DFT) was employed in all computations. The core electrons are described using the projector-augmented-wave (PAW) method. The exchange-correlation effect was estimated by Generalized Gradient Approximation Perdew–Burke–Ernzerhof (GGA-PBE) functionals. The plane wave energy cutoff was set as 450 eV. All structures were optimized until the energy and force reached the convergence thresholds of 10^{-4} eV and -0.02eV/ Å, respectively. A Monkhorst-Pack k-mesh with a 3 × 3 × 1 k-point grid was used for structural optimization and frequency, while 6 × 6 × 1 for high-quality electronic analysis. The vacuum slab was set to 20.0 Å to avoid interactions between neighboring supercells. The DFT-D3 method was involved to describe the van der Waals interaction. The Gibbs free energy change (ΔG) involved in each elementary reaction calculation was in terms of the computational hydrogen electrode model proposed by Nørskov et al. The calculation formula is:

$$\Delta G = \Delta E + \Delta ZPE - T\Delta S + eU + \Delta G_{pH}$$

where, ΔE is the DFT-calculated reaction energy in a vacuum, T is set to 298.15 K and the entropy S is computed by fixing the catalyst base as the premise. U is the electrode potential versus reversible hydrogen electrode (RHE). ΔG_{pH} is the correction applied to the pH value in the electrolyte that equals $k_B T \times \ln 10 \times pH$.

Assembly of the zinc-nitrate battery and electrochemical test

The zinc-nitrate battery was assembled with carbon paper (1×1 cm^2, catalyst loading was 1mg cm^{-2}) as the working electrode and zinc plate (2×2 cm^2) as the both reference and counter electrodes. All the tests were performed in a H-type cell with 20 mL of cathode electrolyte (1 M KOH + 0.05 M KNO_3) and 20 mL of anode electrolyte (1 M KOH). The bipolar membrane was used to separate the cathodic and anodic electrolytes.

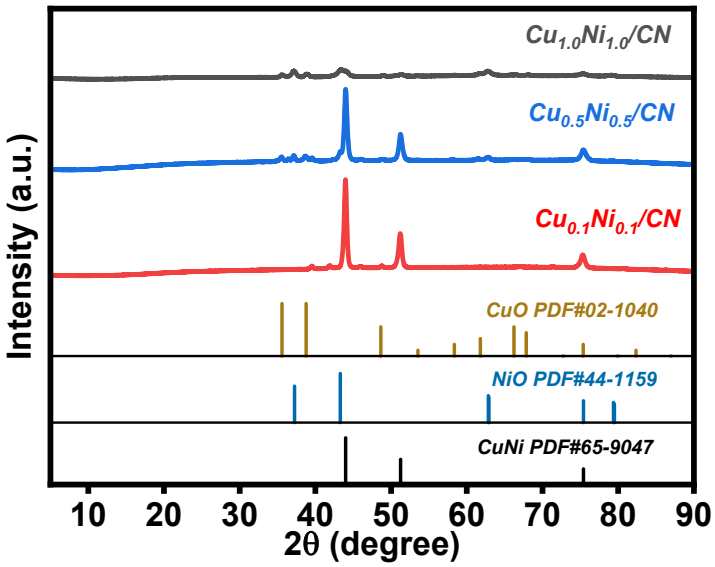

Figure S1. XRD patterns of catalysts $Cu_{0.1}Ni_{0.1}$/CN, $Cu_{0.5}Ni_{0.5}$/CN and $Cu_{1.0}Ni_{1.0}$/CN.

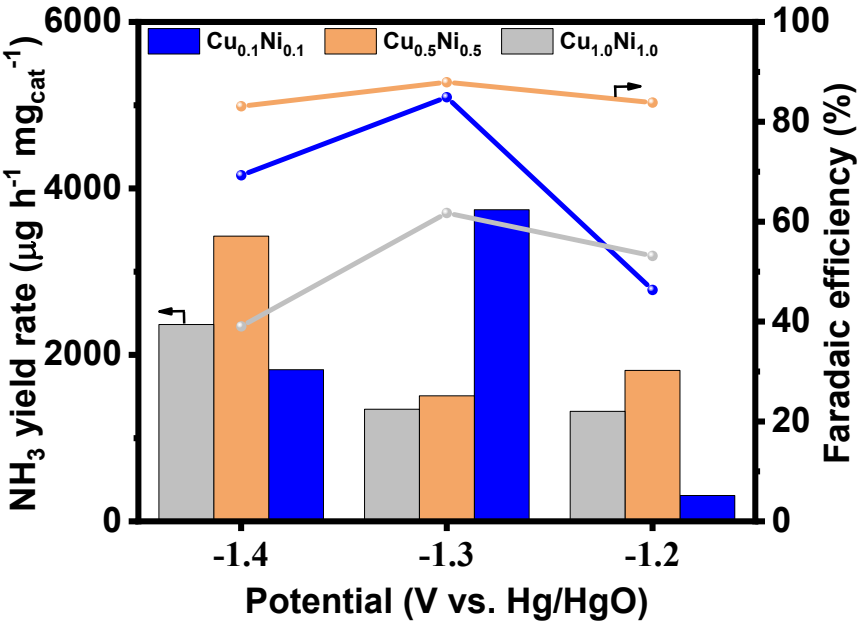

Figure S2. Comparison of the performances of $Cu_{0.1}Ni_{0.1}$/CN, $Cu_{0.5}Ni_{0.5}$/CN and $Cu_{1.0}Ni_{1.0}$/CN catalysts in the vicinity of their optimal potentials.

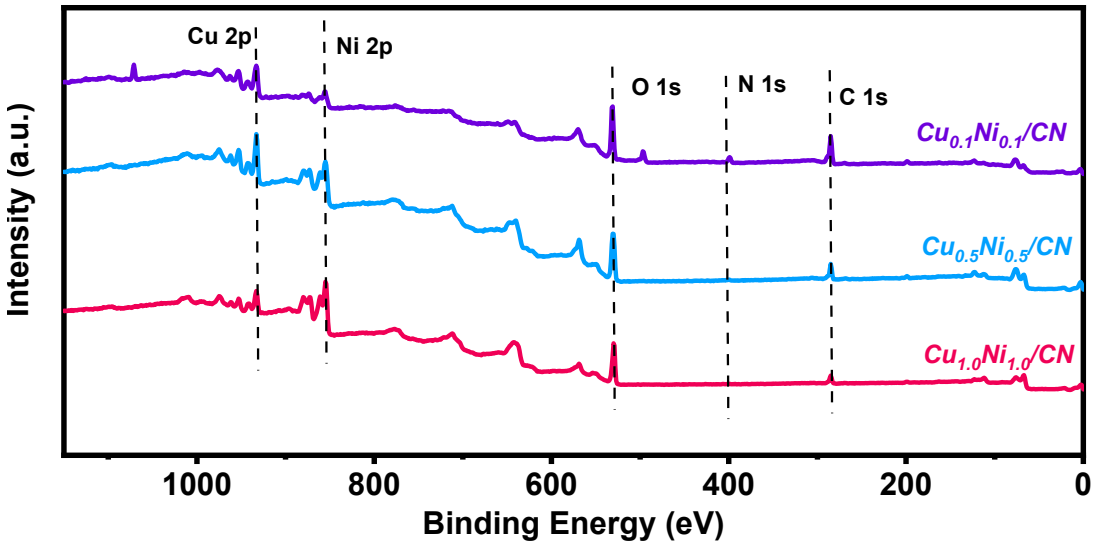

Figure S3. XPS pattern of $Cu_{0.1}Ni_{0.1}$/CN, $Cu_{0.5}Ni_{0.5}$/CN and $Cu_{1.0}Ni_{1.0}$/CN.

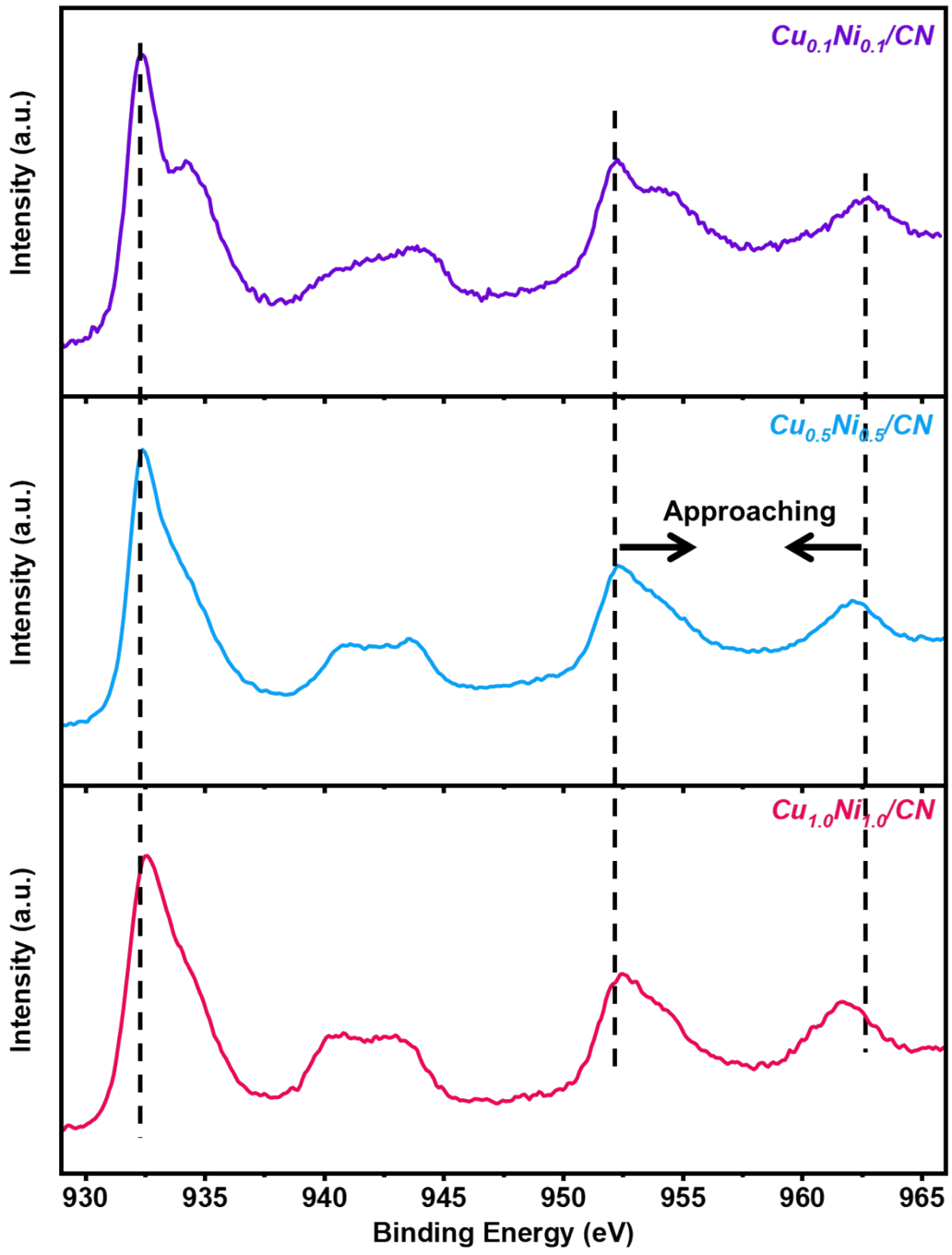

Figure S4. Cu 2p XPS patterns of $Cu_{0.1}Ni_{0.1}$/CN, $Cu_{0.5}Ni_{0.5}$/CN and $Cu_{1.0}Ni_{1.0}$/CN.

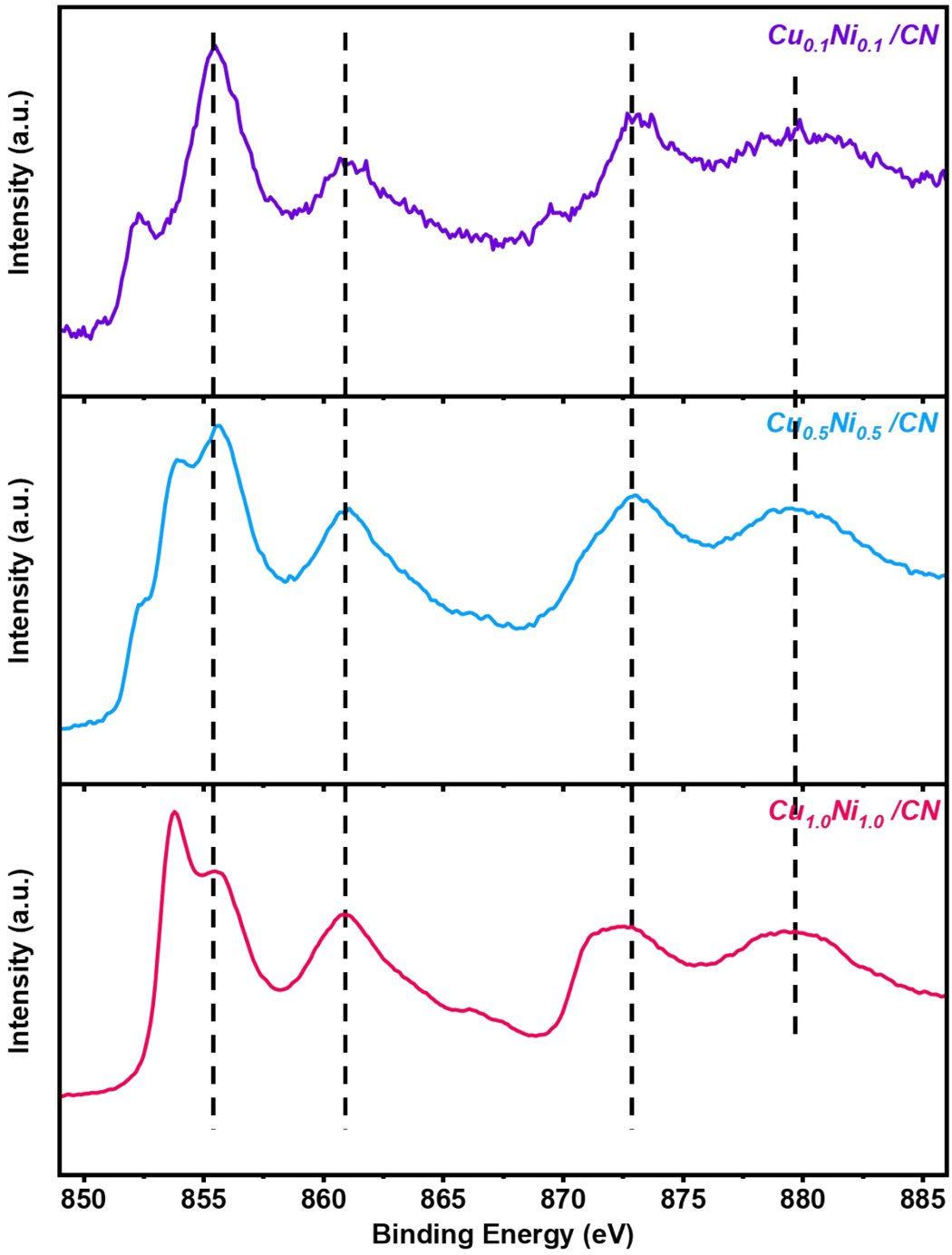

Figure S5. Ni 2p XPS patterns of $Cu_{0.1}Ni_{0.1}$/CN, $Cu_{0.5}Ni_{0.5}$/CN and $Cu_{1.0}Ni_{1.0}$/CN.

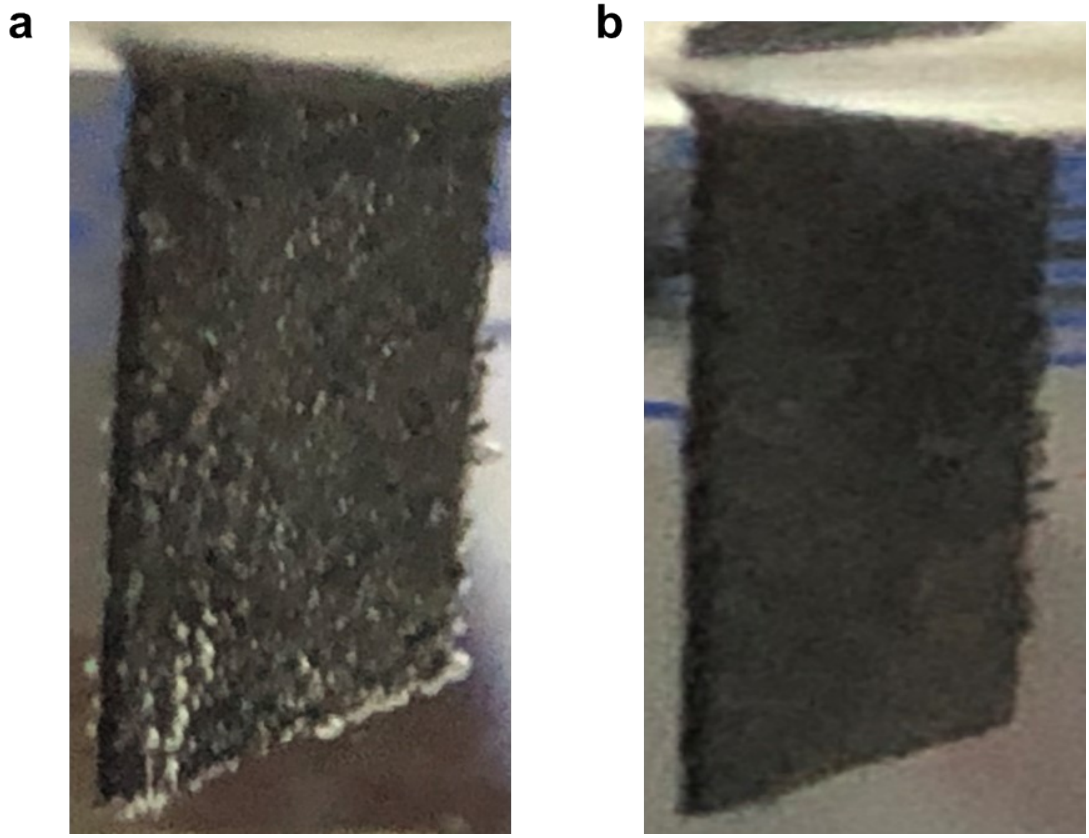

Figure S6. Surface phenomena of the working electrode. (a) Vigorous hydrogen evolution reaction dominating after -1.3 V. (b) Nitrate reduction dominating before -1.3 V.

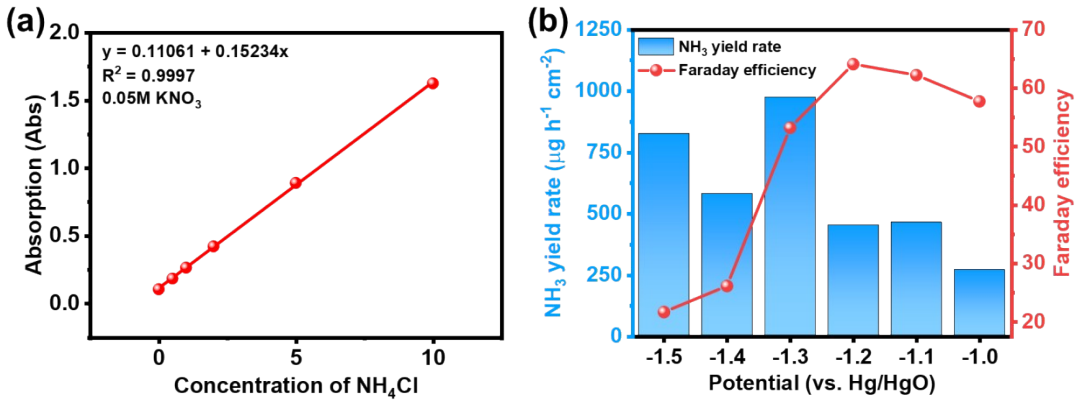

Figure S7. Performance of $Cu_{0.5}Ni_{0.5}$/CN under 1.0 M KOH containing 0.05 M KNO_3. (a) Standard curve of NH_4Cl in 0.05 M KNO_3 and 1.0 M KOH electrolyte. (b) Ammonia yield rate and faradaic efficiency of $Cu_{0.5}Ni_{0.5}$/CN catalyst in 0.05 M KNO_3 and 1.0 M KOH electrolyte under -1.0 V to -1.5 V (vs. Hg/HgO).

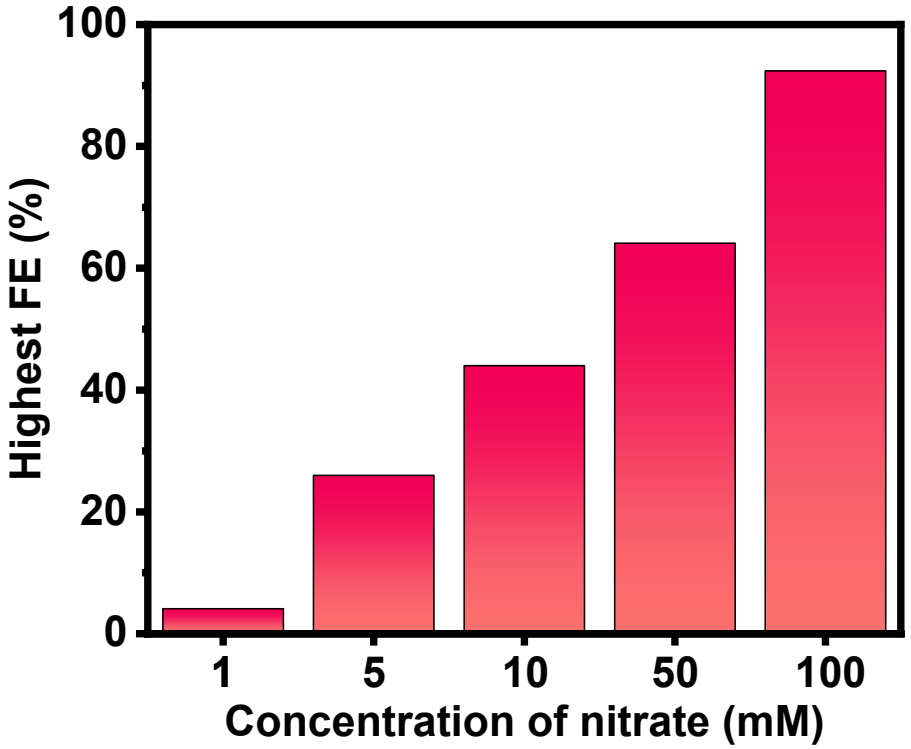

Figure S8. The highest FE of $Cu_{0.5}Ni_{0.5}$/CN in 1.0 M KOH containing different concentrations of nitrate.

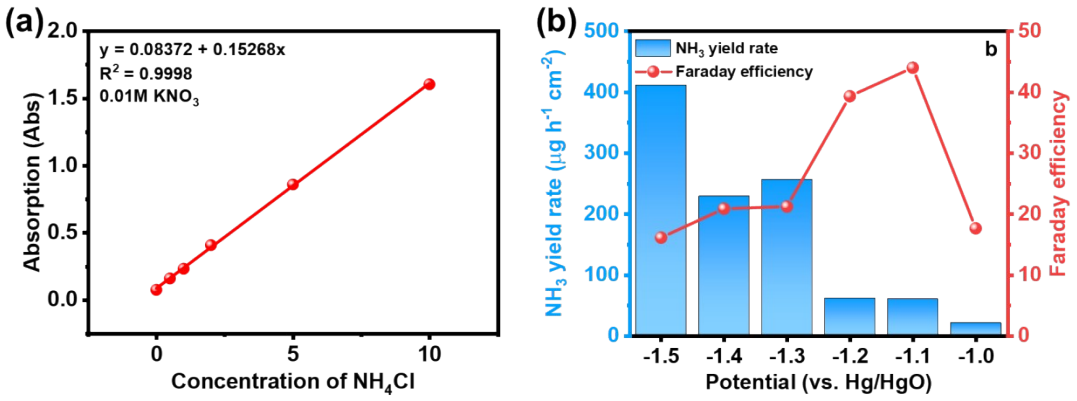

Figure S9. Performance of $Cu_{0.5}Ni_{0.5}$/CN under 1.0 M KOH containing 0.01 M KNO_3. (a) Standard curve of NH_4Cl in 0.01 M KNO_3 and 1.0 M KOH electrolyte. (b) Ammonia yield rate and faradaic efficiency of $Cu_{0.5}Ni_{0.5}$/CN catalyst in 0.01 M KNO_3 and 1.0 M KOH electrolyte under -1.0 V to -1.5 V (vs. Hg/HgO).

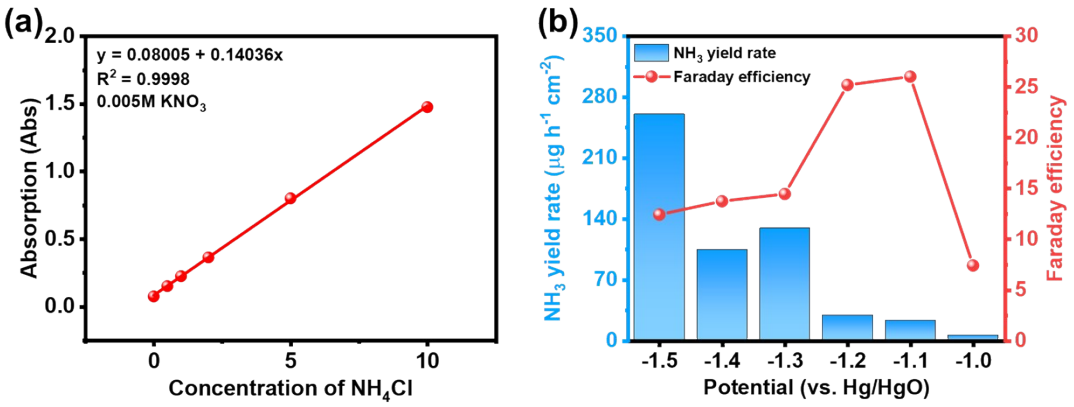

Figure S10. Performance of $Cu_{0.5}Ni_{0.5}$/CN under 1.0 M KOH containing 0.005 M KNO_3. (a) Standard curve of NH_4Cl in 0.005 M KNO_3 and 1.0 M KOH electrolyte. (b) Ammonia yield rate and faradaic efficiency of $Cu_{0.5}Ni_{0.5}$/CN catalyst in 0.005 M KNO_3 and 1.0 M KOH electrolyte under -1.0 V to -1.5 V (vs. Hg/HgO).

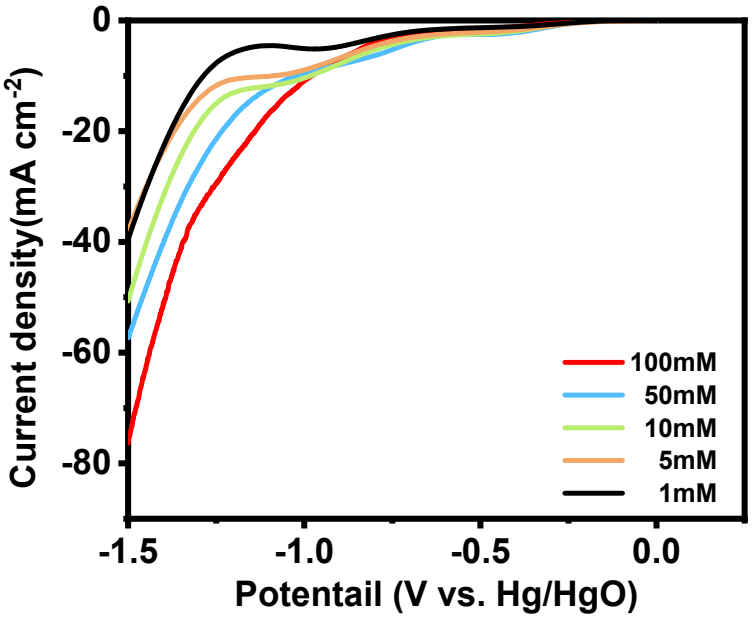

Figure S11. LSV curves of electrolytes containing different concentration NO_3^-.

Table S1. Comparison of NO_3^-RR performance of non-precious catalysts in this work and in the literature

Catalysts	Electrocatalytic conditions	Power supply	NH_3 faradaic efficiency (%)	Ref.
$Cu_{6h,Air}$	1.0 M NaOH + 100 mM $NaNO_3$	-0.38 V (vs. RHE)	79	1
Cu20-Pd80	1.0 M NaOH + 100 mM $NaNO_3$	−0.01 V (vs. RHE)	87	2
Cu_{upd}/Pt_{NSF}	0.1 M NaOH + 100 mM $NaNO_3$	+ 0.15 V (vs. RHE)	<10	3
Ti	0.3 M KNO_3+ 0.1 M HNO_3	−1.0 V (vs. RHE)	82	4
Pd (1 1 1)	0.5 M Na_2SO_4 + 100 mM NO_3^-	0.7 V (vs. RHE)	79.91	5
Cu@ZrO_2	100 ppm NO_3^--N +0.1 M Na_2SO_4	−0.7 V (vs. RHE)	67.6	6
Cu_7Ni_3/OMC	0.1 M PBS+ 0.1 M $NaNO_3$	−0.8 V (vs RHE)	78.9	7
PTCDA/O-Cu	0.1 M PBS+ 500 ppm KNO_3	−0.4 V (vs RHE)	85.9	8
Cu/Cu_2O NWAs	0.5 M Na_2SO_4 + 100 ppm NO_3^--N	−0.85 V (vs RHE)	81.2	9
Cu@$Cu_{2+1}O$ NWs	0.5 M K_2SO_4 + 50 mg L^{-1} NO_3^-	−0.5 V (vs. RHE)	87.07	10
R-Cu_2O/Cu/CF	1 M KOH + 250 mg L^{-1} NO_3^-	−0.25 V (vs. RHE)	84.36	11
Co_3O_4/Ti	0.1 M Na_2SO_4 + 50 mg L^{-1} NO_3^-	10 mA cm^{-2}	80	12
OD-Ag	0.1 M KCl + 100 mM NO_3^-	−0.72 V (vs. RHE)	89	13
Co/CoO NSAs	0.1 M Na_2SO_4 + 200 ppm NO_3^--N	−0.64 V (vs. RHE)	91.2	14
$Cu_{0.5}Ni_{0.5}$/CN	1 M KOH + 100 mM KNO_3	−0.38 V (vs. RHE)	92.4	This work

References:

1. D. Reyter, G. Chamoulaud, D. Bélanger and L. Roué, *Journal of Electroanalytical Chemistry*, 2006, **596**, 13-24.
2. D. Reyter, D. Belanger and L. Roue, *The Journal of Physical Chemistry C*, 2009, **113**, 290-297.
3. C. Roy, J. Deschamps, M. Martin, E. Bertin, D. Reyter, S. Garbarino, L. Roué and D. Guay, *Applied Catalysis B: Environmental*, 2016, **187**, 399-407.
4. J. M. McEnaney, S. J. Blair, A. C. Nielander, J. A. Schwalbe, D. M. Koshy, M. Cargnello and T. F. Jaramillo, *ACS sustainable chemistry & engineering*, 2020, **8**, 2672-2681.
5. Y. Han, X. Zhang, W. Cai, H. Zhao, Y. Zhang, Y. Sun, Z. Hu, S. Li, J. Lai and L. Wang, *Journal of Colloid and Interface Science*, 2021, **600**, 620-628.
6. J. Xia, H. Du, S. Dong, Y. Luo, Q. Liu, J. S. Chen, H. Guo and T. Li, *Chemical Communications*, 2022, **58**, 13811-13814.
7. J. Zhao, L. Liu, Y. Yang, D. Liu, X. Peng, S. Liang and L. Jiang, *ACS Sustainable Chemistry & Engineering*, 2023, **11**, 2468-2475.
8. G.-F. Chen, Y. Yuan, H. Jiang, S.-Y. Ren, L.-X. Ding, L. Ma, T. Wu, J. Lu and H. Wang, *Nature Energy*, 2020, **5**, 605-613.
9. Y. Wang, W. Zhou, R. Jia, Y. Yu and B. Zhang, *Angewandte chemie international edition*, 2020, **59**, 5350-5354.
10. T. Ren, K. Ren, M. Wang, M. Liu, Z. Wang, H. Wang, X. Li, L. Wang and Y. Xu, *Chemical Engineering Journal*, 2021, **426**, 130759.
11. W. Fu, Z. Hu, Y. Zheng, P. Su, Q. Zhang, Y. Jiao and M. Zhou, *Chemical Engineering Journal*, 2022, **433**, 133680.
12. J. Gao, B. Jiang, C. Ni, Y. Qi, Y. Zhang, N. Oturan and M. A. Oturan, *Applied Catalysis B: Environmental*, 2019, **254**, 391-402.
13. H. Liu, J. Park, Y. Chen, Y. Qiu, Y. Cheng, K. Srivastava, S. Gu, B. H. Shanks, L. T. Roling and W. Li, *ACS Catalysis*, 2021, **11**, 8431-8442.
14. Y. Yu, C. Wang, Y. Yu, Y. Wang and B. Zhang, *Science China Chemistry*, 2020, **63**, 1469-1476.